Journal of Materials Chemistry A

Accepted Manuscript

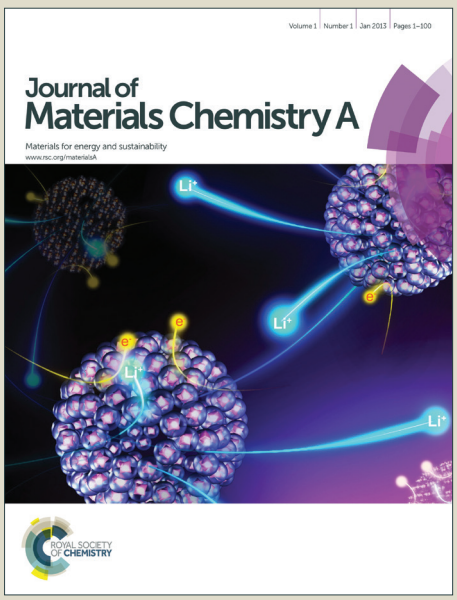

This is an *Accepted Manuscript*, which has been through the Royal Society of Chemistry peer review process and has been accepted for publication.

Accepted Manuscripts are published online shortly after acceptance, before technical editing, formatting and proof reading. Using this free service, authors can make their results available to the community, in citable form, before we publish the edited article. We will replace this *Accepted Manuscript* with the edited and formatted *Advance Article* as soon as it is available.

You can find more information about *Accepted Manuscripts* in the Information for Authors.

Please note that technical editing may introduce minor changes to the text and/or graphics, which may alter content. The journal's standard Terms & Conditions and the Ethical guidelines still apply. In no event shall the Royal Society of Chemistry be held responsible for any errors or omissions in this *Accepted Manuscript* or any consequences arising from the use of any information it contains.

ROYAL SOCIETY OF CHEMISTRY

www.rsc.org/materialsA

Reaction Kinetics of the Electrochemical Oxidation of CO and Syngas Fuels on a $Sr_2Fe_{1.5}Mo_{0.5}O_{6-\delta}$ Perovskite Anode

Salai Cheettu Ammal[1] and Andreas Heyden[1,*]

ABSTRACT

The performance of a $Sr_2Fe_{1.5}Mo_{0.5}O_{6-\delta}$ (SFMO) perovskite anode has been investigated under solid oxide fuel cell conditions while operating on CO and syngas fuels using periodic density functional theory and microkinetic modeling. Three surface models with different Fe/Mo ratios and oxygen vacancies on the gas exposed surface layer are used to identify the active site and electro-oxidation mechanism for CO and a mixture of CO and H_2. Calculated current densities suggest that SFMO anodes exhibit lower performance while operating on CO compared to H_2 fuel and a surface with a higher Mo concentration in the top most layer exhibits a higher activity for both fuels. Furthermore, the model predicts that desorption of CO_2 and formation of an oxygen vacancy, which is found to be the charge transfer step, is rate-controlling for CO electro-oxidation at operating voltage. The CO oxidation activity can thus be improved by increasing the Mo content or by adding small amounts of an active transition metal on the surface that facilitates the oxygen vacancy formation process by delocalizing the electrons at the vacant site. In the presence of a mixture of CO, H_2 and H_2O gas, the water-gas shift reaction ($CO + H_2O \rightleftharpoons CO_2 + H_2$) is rapid at operating voltage and H_2 electro-oxidation contributes mostly to the overall observed electrochemical activity, while CO is primarily chemically oxidized to CO_2. A higher Mo content in the SFMO surface promotes again a higher activity for syngas fuels with high CO content.

*Corresponding author: email: heyden@cec.sc.edu
[1]*Department of Chemical Engineering, University of South Carolina, 301 Main Street, Columbia, South Carolina 29208, USA*

Journal of Materials Chemistry A Accepted Manuscript

1. Introduction

Solid oxide fuel cells (SOFCs) are among the most promising power generation devices due to their high fuel-to-electricity conversion efficiency and low pollutant emissions.[1] SOFCs operate at high temperatures, typically above 800 °C, which not only offers high electrical efficiency but also fuel flexibility which potentially contributes to better economics. For example, the high fuel flexibility of SOFCs presents advantages over other types of fuel cells such as polymer electrolyte membrane fuel cells (PEMFCs) in that it is possible to use relatively cheap, safe, and readily available carbon-based fuels in addition to hydrogen. Carbon monoxide present in such fuels, e.g., coal gas and synfuels, is not only harmless to SOFCs, but it can also act as a fuel. In addition, CO_2 capture in SOFC-based systems is less expensive and less complex than in conventional combustion systems because the fuel and oxidizer in SOFCs are not in direct contact with each other and thus, do not require expensive gas-separation technologies.[2, 3] Despite the advantages and apparent promise of SOFCs as an efficient energy conversion technology, full scale commercialization of SOFCs is impeded by several obstacles such as improving efficiencies and tolerance to fuel impurities, long-term performance and durability, sealing problems, and overall production costs.

A single SOFC consists of an anode and a cathode separated by a solid oxide electrolyte. Although the long term cell performance can be affected by losses from any of these components, the anodic loss contributes significantly to the overall cell performance whenever carbon based fuels instead of pure hydrogen are used. Thus, fundamental understanding of the elementary reaction steps and kinetics of the electrochemical reactions occurring at the anode becomes essential for further improvement of SOFC performance. Since hydrocarbon fuels such as methane and propane are partially or completely reformed in the porous catalytic anodes,

Journal of Materials Chemistry A Accepted Manuscript

regardless of initial fuel composition the major species involved in the current-producing reactions at the anode are likely related to the H_2 and CO electro-oxidation. In other words, knowledge of the H_2 and CO electro-oxidation mechanism is a necessary prerequisite for understanding the electrochemical performance of SOFCs operating on various hydrocarbon fuels.

The reaction kinetics of the H_2 electro-oxidation has been widely studied on conventional Ni/YSZ (yttria-stabilized zirocinia) anodes and the overall findings have been summarized in a recent review.[4] However, only few studies have investigated the electro-oxidation mechanism of CO and syngas fuels at the Ni/YSZ anode.[5-14] In these studies, it has been shown that the electrochemical reaction rate of CO is lower than that of H_2 possibly due to a larger diffusion resistance of CO on the electrode surface.[7, 11-13] When both H_2 and CO are present in the fuel stream, H_2O produced from the electrochemical oxidation of H_2 can react with CO through the water-gas shift ($CO + H_2O \rightleftharpoons CO_2 + H_2$, WGS) reaction to produce more H_2 and CO_2. Thus, a high performance can still be achieved with a H_2-CO mixture as long as the H_2 content in the fuel stream is greater than 50%.[11] Although these studies provide some understanding on how syngas composition and the presence of reaction products affects the performance of Ni-based SOFC anodes, very little is known about how these factors affect the performance of other alternative anodes based on perovskite oxides that have recently been proposed. In our recent work, we investigated the electrochemical oxidation mechanism of H_2 on the $Sr_2Fe_{1.5}Mo_{0.5}O_{6-\delta}$ (SFMO) perovskite surface, which has been proposed as a promising alternative anode for SOFCs, using periodic density functional theory (DFT) calculations and microkinetic modeling techniques.[15] Herein, we investigate the kinetics of the electrochemical reactions on our SFMO surface models using CO and syngas fuels.

Journal of Materials Chemistry A Accepted Manuscript

Recent studies reported that the SFMO perovskite material exhibits the characteristic behavior of a mixed ionic and electronic conductor while possessing significant electrocatalytic activity for H_2 fuel and natural gas with high tolerance to sulfur and carbon deposition.[16-21] While the electronic conductivity of SFMO is promoted by the presence of mixed-valent Mo^{5+}/Mo^{6+} and Fe^{3+}/Fe^{4+}, its high ionic conductivity originates from a high oxygen vacancy concentration as well as low oxygen ion migration barriers.[18, 19] Next, experimental studies reported that SFMO displays a good thermal compatibility with the $La_{0.9}Sr_{0.1}Ga_{0.8}Mg_{0.2}O_{3-\delta}$ (LSGM) electrolyte and can process H_2 and hydrocarbon fuels with good sulfur tolerance.[16, 17] However, the electro-catalytic activity of SFMO is low compared to the conventional Ni anodes, which leads to an overall low cell performance. Finally, experimental studies suggested that the dispersion of a small amount of Ni (~2 wt%) can significantly improve the performance of cells operating on H_2 and CH_4 fuels, suggesting that anode performance is at least partially performance controlling.[17, 21]

In our recent computational study, we investigated the H_2 electro-oxidation mechanism on the SFMO (001) surface models possessing different Fe/Mo ratios on the surface.[15] We identified that the SFMO surface with a higher Mo concentration on the gas exposed layer exhibits a higher activity towards H_2 oxidation; however, the surface Mo concentration tends to be very low under SOFC operating conditions. In agreement with experimental reports,[17, 21] our calculations also suggested that the rate-controlling surface oxygen vacancy formation process can be promoted by adding small Ni particles on the least active (but most stable under operating conditions) FeO_2-terminated SFMO surface. A similar approach is used in the present study to investigate the electro-oxidation mechanism of CO on the SFMO surface. Once the rates of CO oxidation are calculated and the rate-controlling steps are identified, we further examined the

Journal of Materials Chemistry A Accepted Manuscript

oxidation kinetics of a CO/H_2 mixture on the SFMO surfaces. The goal of this study is to compare the relative performance of SOFCs with Ni/YSZ (from literature) and SFMO anodes while operating on H_2, CO, and syngas fuels and to evaluate how the partial pressure of the fuel species and reaction products affect the overall cell performance. In addition, a computational framework is presented that permits concurrent simulation of chemical (e.g. the water-gas shift) and electro-chemical (H_2 and CO oxidation) processes on an electrode surface under steady state operating conditions. Finally, we note that for hydrocarbon fuels such as methane C-H bond dissociations and carbon deposition constitute anode performance limiting factors that are beyond this study but that we will address in a future publication. Also, the Boudouard reaction ($2CO \rightleftharpoons CO_2 + C \downarrow$) is not considered here but will be investigated in the context of a coking study of SFMO.

2. Computational Model and Methods

The SFMO (001) surface models used in the present study have been created from optimized lattice parameters of a *Fm3m* cubic SFMO structure. The crystallographic data of SFMO and a detailed surface model development procedure are provided in the supporting information as well as in our recent work.[15] The bulk SFMO structure can have two different configurations where the Mo atoms are distributed in a planar or diagonal orientation. From these two bulk structures, three different surface models are created, namely a "plane-Mo" surface, "diagonal-Mo" surface, and a FeO_2-terminated surface (Figure 1). We have shown in our earlier work that these asymmetric slab models with a dipole correction scheme can predict reaction energies reasonably well compared to symmetric slab models.[15] Each SFMO (001) slab has four SrO and four $Fe(Mo)O_2$ layers and the reaction mechanism was examined only on the $Fe(Mo)O_2$ terminated layer, i.e., we assume that the A-terminated SrO layer is not catalytically

Journal of Materials Chemistry A Accepted Manuscript

active. Since SOFCs are operated at high temperatures (>1000 K) and reducing conditions (low oxygen partial pressures), multiple oxygen vacancies are expected to be present in the SFMO material. Thus, we sequentially created multiple oxygen vacancies by identifying the lowest energy structure at different vacancy concentration. Constrained *ab initio* thermodynamic analysis suggested that under SOFC operating conditions (P_{O2} = 10^{-20} atm, T = 1100 K), all the three surface models possess five oxygen vacancies although the distribution of oxygen vacancies are different among the three surface models. On the top-most surface layer, the "plane-Mo" surface has two Mo atoms and two oxygen vacancies (Figure 1a), the "diagonal-Mo" surface has one Mo atom and three oxygen vacancies (Figure 1b), and the FeO_2-terminated surface has no Mo atom and four oxygen vacancies (Figure 1c). Since the fuel oxidation occurs on the top surface layer, different configurations of this layer in the three surface models allow us to identify the effect of Mo concentration as well as different oxidation states of Fe on the catalytic activity of SFMO.

Journal of Materials Chemistry A Accepted Manuscript

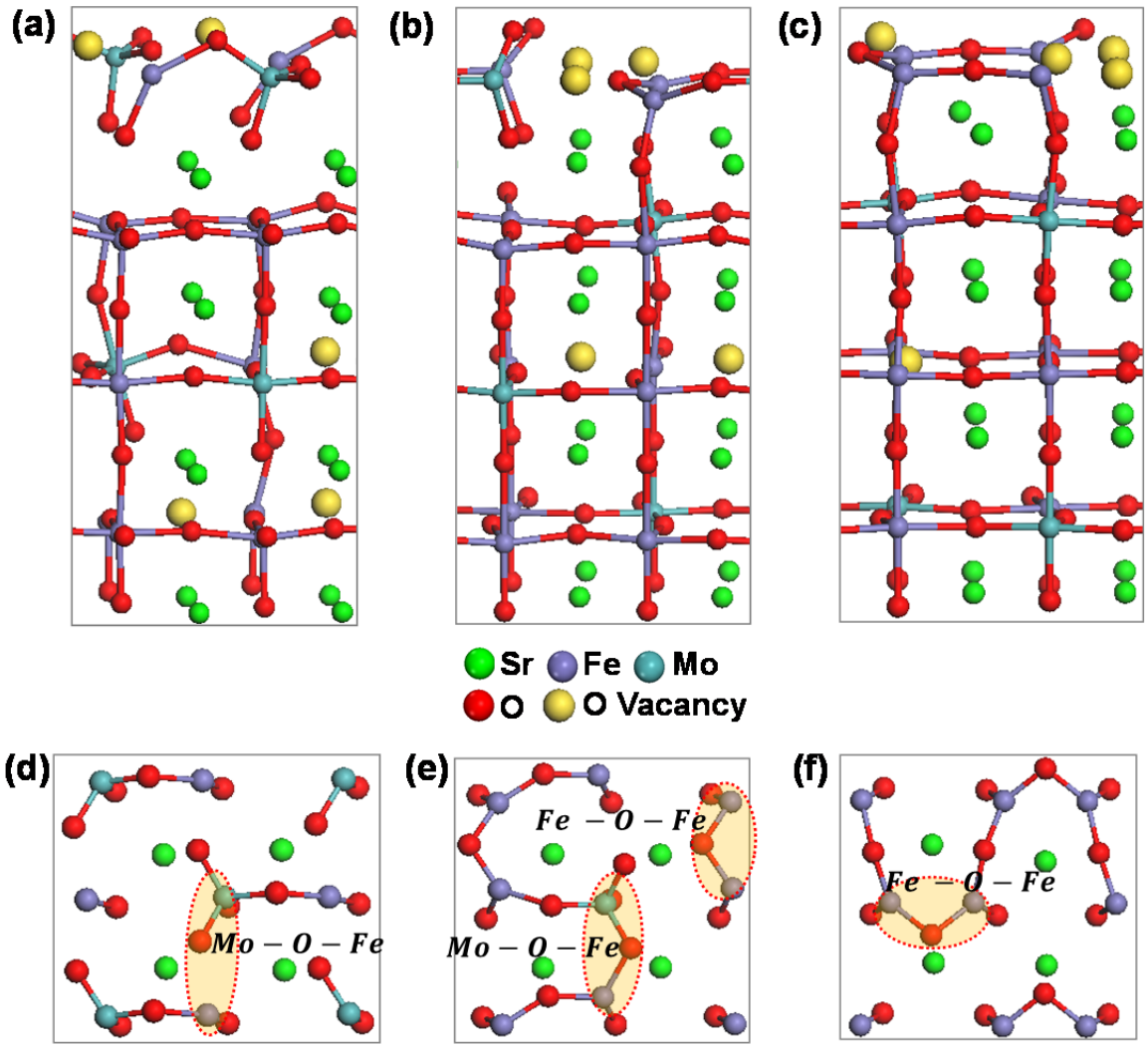

Figure 1 $Sr_2Fe_{1.5}Mo_{0.5}O_{6-\delta}$ (δ=0.625) (001) surface models used to investigate the CO electro-oxidation mechanism. (a) & (d) side and top views of "plane-Mo" surface (Mo:Fe = 1), (b) & (e) side and top views of "diagonal-Mo" surface (Mo:Fe = 0.33), (c) & (f) side and top views of FeO_2-terminated surface (Mo:Fe = 0). Highlighted areas correspond to the active sites considered for CO oxidation.

The periodic slab plane wave calculations presented in this work were carried out with the Vienna Ab initio Simulation Package (VASP 5.3).[22, 23] The electronic structures of SFMO surfaces were modeled on the basis of spin-polarized DFT+*U* theory,[24-27] which minimizes the self-interaction error inherent in pure DFT when applied to transition metals with tightly localized d-electrons, such as Fe in SFMO. The generalized gradient approximation (GGA) with the Perdew-Burke-Ernzerhof (PBE)[28] functional was used to describe exchange and correlation

Journal of Materials Chemistry A Accepted Manuscript

effects. All-electron frozen core projector augmented-wave (PAW) potentials[29] were employed to describe the nuclei and core electronic states while the Sr 4s4p5s, Fe 3p3d4s, Mo 4p5s4d, O 2s2p, and C 2s2p were treated as valence electrons. The wavefunctions were expanded in plane waves, defined by a kinetic energy cutoff of 800 eV. Integration of properties over the first Brillouin zone was performed via the Monkhorst-pack (MP)[30] *k*-point sampling scheme. A 4×4×1 *k*-point mesh and a Gaussian smearing finite temperature broadening method (σ = 0.05 eV) were used during structural relaxations. The bottom-most layer was fixed in all calculations to mimic a semi-infinite bulk crystal and a vacuum gap of 15 Å was used to minimize the interaction between images along the z-axis. Dipole and quadrupole corrections to the energy are taken into account using a modified version of the Markov and Payne method,[31] in which the total energy is corrected for the contribution of dipole interactions along the z-axis. We used a U-J value of 4.0 eV for Fe d-electrons and no U-J parameter for Mo based on earlier computational studies of SFMO.[18,32] We find that the antiferromagnetic arrangement of Fe spins is the most stable arrangement in all of the three surface configurations. The climbing image nudge-elastic band (CI-NEB)[33] and dimer methods[34-36] were used to optimize the transition state (TS) structures of various elementary steps.

The molecular level information obtained from the DFT+*U* calculations were linked to macroscopic physical and chemical phenomena such as, reaction rates, product yields, and selectivities with the help of microkinetic modeling. Details of the microkinetic model used in the present study are provided in the supporting information. Overall, we followed a similar approach to the one used for the H_2 electro-oxidation mechanism.[15] Next, the PBE functional used here is known to underestimate the gas phase energy of the CO molecule and in turn overestimates the gas phase reaction enthalpies of reactions involving a CO molecule.[37, 38] As

Journal of Materials Chemistry A Accepted Manuscript

already previously reported by Peterson et al.,[37] we performed a statistical analysis of a set of gas phase reactions, including CO, CO_2, H_2, and H_2O and identified that the error is likely centered on the CO molecule and is -0.42 eV for our current computational setup. We added this correction to the calculated gas phase energy of the CO molecule in order to make a reasonable comparison between H_2 and CO oxidation reactions. Harmonic transition state theory and collision theory (sticking coefficient = 1) were used to calculate rate constants for elementary surface reactions and adsorption processes, respectively. The active surface area considered in our present calculations is equal to 6.20×10^{-19} m^2. We calculated the zero-point energy (ZPE = $\sum_i \frac{1}{2} h\upsilon_i$) from the normal mode frequencies, υ_i, determined from the eigenvalues of the Hessian. Displacements of ±0.02 Å were used along the x, y, and z directions to construct the Hessian matrix from analytic gradients. The atoms displaced during the frequency calculations are the adsorbed gas species and the nearest neighbor atoms of the catalytic site on the SFMO surface model. After calculating the forward and reverse rate constants for each elementary step, we constructed a master equation and solved it using the BzzMath library developed by Buzzi-Ferraris.[39] The steady-state solution provides a probability density for the system to occupy each discrete state and these probability densities are referred to in the following as surface coverages, θ. The reaction rate (turn over frequency) of each pathway was then calculated using these surface coverages. For syngas fuel, we combined the elementary steps of the H_2 and CO electro-oxidation reactions in the microkinetic model for the current calculation. Campbell's degree of rate control and degree of thermodynamic rate control analyses[40, 41,42, 43] were employed to identify the rate-controlling steps and the most important reaction intermediates.

3. Results and Discussion

Journal of Materials Chemistry A Accepted Manuscript

3.1. CO Oxidation Mechanism on SFMO (001) Surfaces.

The different Fe/Mo ratios on the top layer of the three surface models offer different types of active sites, such as $Mo-O-Fe$ and/or $Fe-O-Fe$ on each surface for the CO electro-oxidation as shown in Figures 1(d)-1(f). While we have only $Mo-O-Fe$ type oxygen atoms on the "plane-Mo" surface and only $Fe-O-Fe$ type oxygen atoms on the FeO_2-terminated surface, the "diagonal-Mo" surface possess both types of oxygen atoms. In our earlier work, we identified that the H_2 oxidation activity at $Fe-O-Fe$ sites of the "diagonal-Mo" surface is very similar to that of the FeO_2-terminated surface.[15] Bader charge analysis further confirmed that the oxidation state of Fe atoms at the $Fe-O-Fe$ site of both diagonal-Mo and FeO_2-terminated surfaces are very similar (+2, formal charges). As a result, we expect a similar trend for the CO oxidation activity at the $Fe-O-Fe$ sites of these two surfaces and thus, investigated the CO oxidation mechanism only on the $Mo-O-Fe$ site of the "diagonal-Mo" surface. Equation (1) describes the overall electrochemical oxidation of CO at the SFMO anode in Kröger-Vink notation.[44]

$$CO_{(g)} + O_O^{\times}(SFMO) \rightarrow CO_{2(g)} + 2e' + V_O^{\bullet\bullet}(SFMO) \qquad (1)$$

Here, $O_O^{\times}$ denotes the neutral oxygen atom on the SFMO surface and $V_O^{\bullet\bullet}$corresponds to a positively charged oxygen vacancy on the surface. The two electrons removed from the surface oxygen atom during the oxidation process are transferred via the $M-O-Fe$ (M = Mo or Fe) bridge to the current collector. The elementary reaction steps of this CO oxidation process (not including the electron transfer) at an active site $*_M-O-Fe$ (M = Mo or Fe) are described in reactions (R1) to (R4).

$$*_M-O-Fe\ (IM1) + CO_{(g)} \rightarrow CO_M-O-Fe\ (IM2) \qquad (R1)$$

$$CO_M-O-Fe\ (IM2) \rightarrow OCO_M-Fe\ (IM3) \qquad (R2)$$

Journal of Materials Chemistry A Accepted Manuscript

$$OCO_{M} - Fe\ (IM3) \rightarrow *_{M} - V_{O}(S) - CO_{2\,(Fe)}\ (IM4) \qquad (R3)$$

$$*_{M} - V_{O}(S) - CO_{2\,(Fe)}\ (IM4) \rightarrow *_{M} - V_{O}(S) - Fe\ (IM5) + CO_{2\,(g)} \qquad (R4)$$

In the first elementary step (R1), a CO molecule adsorbs on a metal site (Mo or Fe) which further reacts with the neighboring oxygen atom (R2) forming a bridged structure where CO is bridge bonded between the metal and oxygen atoms. In the following step (R3), CO_2 is formed by creating a surface oxygen vacancy ($V_O(S)$) and the linear CO_2 molecule is only weakly bonded to the neighboring Fe atom (IM4). Desorption of CO_2 from the SFMO surface is considered in step (R4). While the reaction steps (R1)-(R4) complete the CO oxidation process, the catalytic cycle is not completed until we include the process of oxygen ion migration from the SFMO bulk to the surface oxygen vacancy (R5) and the bulk oxygen vacancy ($V_O(B)$) being filled by an oxygen ion from the cathode (R6). In the following, we assumed that these cathode processes are fast, i.e., the anode reactions are rate controlling, which is at least partially justified since modifying the anode surface with a transition metal, while not changing the cathode, led experimentally to an improved performance.[17, 21]

$$*_{M} - V_{O}(S) - Fe\ (IM5) \rightarrow *_{M} - V_{O}(B) - Fe\ (IM6) \qquad (R5)$$

$$*_{M} - V_{O}(B) - Fe\ (IM6) + \frac{1}{2}O_{2\,(g)} \rightarrow *_{M} - O - Fe\ (IM1) \qquad (R6)$$

The detailed procedure used to calculate the rate of reaction (R6) is explained in the supporting information as well as in our recent work on the H_2 electro-oxidation on SFMO.[15] By assuming that the oxygen reduction rate and current collection at the cathode are fast under SOFC operating conditions, we used the bulk oxygen diffusion barrier of SFMO (0.33 eV)[19] to calculate the rate of reaction (R6). All DFT+*U* calculations presented in this work have been performed on charge neutral surface models and one e^- or two e^- charge transfer steps during at all possible elementary processes are considered in our microkinetic model. In the following, we

Journal of Materials Chemistry A Accepted Manuscript

refrain from using Kröger-Vink notation in eqns. (R1)-(R6) because we found it often not clear at this point when and how (one e^- or two e^-) charge transfer occurs.

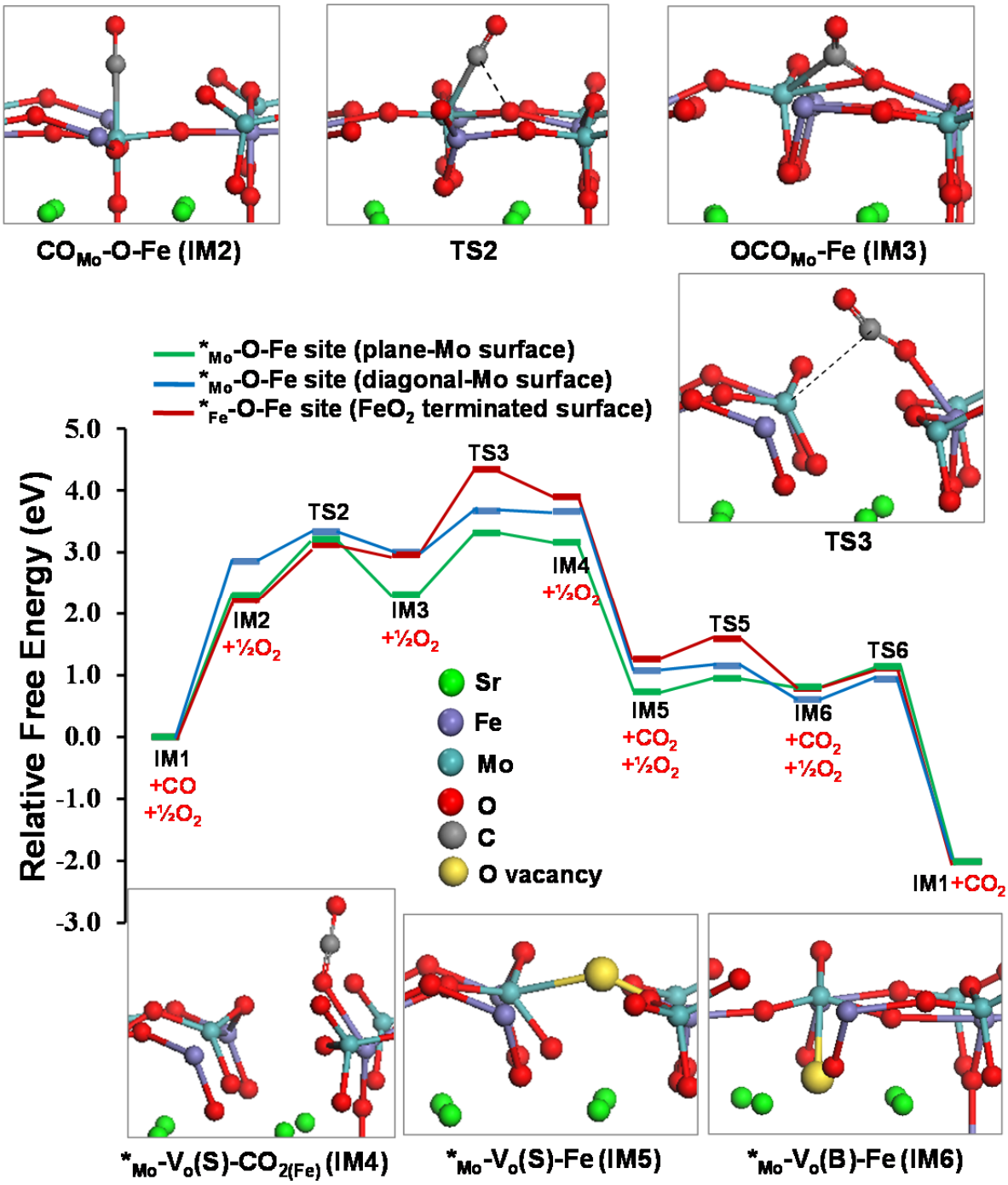

Figure 2. Free energy profiles (eV) for the CO oxidation reaction on the three different surface models of SFMO (T = 1100 K; P_i(gas) = 1 atm). All energies are with reference to the sum of the energies of the initial state (IM1) and the gas phase molecules. The insets provide a side view of the optimized structures of the intermediates and TSs for the "plane-Mo" surface model.

Journal of Materials Chemistry A Accepted Manuscript

Gibbs free energy profiles calculated at T = 1100 K and P_i(gas) = 1 atm for the CO oxidation on the three surface models are shown in Figure 2 and summarized in the supporting information (Table S1). The structures shown in the inset correspond to the intermediates and TS structures calculated on the "plane-Mo" surface ($Mo-O-Fe$ site) model. The optimized structures for the "diagonal-Mo" surface ($Mo-O-Fe$ site) and FeO_2-terminated surface ($Fe-O-Fe$ site) are provided in the supporting information. The TS structures are numbered with reference to the elementary reaction steps (R1 – R6) throughout this paper. The free energy profiles suggest that CO adsorption is slightly favored on the $Fe-O-Fe$ site of the FeO_2-terminated surface (ΔE_{ZPE} = -0.14 eV) compared to the $Mo-O-Fe$ sites of the "plane-Mo" and "diagonal-Mo" surfaces. However, the adsorption is highly endergonic on all the three surface models at a reaction temperature of 1100 K considered here. On the $Mo-O-Fe$ sites of the "plane-Mo" and "diagonal-Mo" surfaces, we considered the adsorption of CO on Mo in step (R1) rather than on Fe atom. Although the CO adsorption on the Fe atom is favored over the Mo atom by about 0.2-0.3 eV on these two surfaces, the transfer/ diffusion of CO from Fe to the neighboring oxygen atom requires much higher barriers than the transfer of CO from Mo to the same oxygen atom. Furthermore, we could not optimize a bridged CO structure similar to IM3 (Figure 2) when CO is adsorbed on Fe. Thus, our reaction pathways on the "plane-Mo" and "diagonal-Mo" surfaces proceed with the initial adsorption of CO on Mo rather than Fe. Considering that we did not find CO adsorption to be rate controlling, this simplification does not affect our overall results. The free energy profiles indicate that the TS structure corresponding to the CO_2 formation process (TS3) is the highest energy state on each surface model and the free energy of the TS increases in the order "plane-Mo" < "diagonal-Mo" < FeO_2-

Journal of Materials Chemistry A Accepted Manuscript

terminated surface. We observed a similar trend for the H_2 electro-oxidation process where the highest energy TS corresponded to either the H-transfer process or the H_2O formation process.[15] In addition, the surface oxygen vacancy formation is favored on the "plane-Mo" surface over the other two surfaces. Overall, the "plane-Mo" surface follows the lowest free energy pathway for the CO oxidation relative to the two other surface models and thus, is expected to be most active.

Table 1. Forward rate constants (k_{for}) and equilibrium constants (K) calculated at a temperature of 1100 K and a standard, reference pressure of 1 atm for each gas species for the elementary steps of the CO oxidation on various SFMO surfaces

Reaction step	plane-Mo surface $*_{Mo}$-O-Fe site		diagonal-Mo surface $*_{Mo}$-O-Fe site		FeO_2-terminated surface $*_{Fe}$-O-Fe site	
	k_{for} (s^{-1})	K	k_{for} (s^{-1})	K	k_{for} (s^{-1})	K
R1	1.70×10^{5}	7.41×10^{-9}	5.82×10^{3}	2.54×10^{-10}	4.27×10^{6}	1.86×10^{-7}
R2	1.69×10^{9}	7.71×10^{-1}	6.79×10^{10}	2.28×10^{-1}	1.66×10^{8}	2.13×10^{-4}
R3	6.55×10^{8}	3.09×10^{-3}	1.91×10^{10}	9.16×10^{-3}	6.39×10^{7}	4.69×10^{-4}
R4	2.29×10^{13}	8.80×10^{5}	2.29×10^{13}	3.65×10^{6}	2.29×10^{13}	7.61×10^{6}
R5	4.20×10^{11}	4.20×10^{-1}	2.34×10^{12}	2.30×10^{2}	2.57×10^{11}	6.41×10^{1}
R6	6.76×10^{11}	2.52×10^{14}	6.76×10^{11}	3.70×10^{12}	6.76×10^{11}	1.82×10^{14}

The reaction free energies, activation barriers, entropies of surface intermediates, and frequency factors of the six elementary steps (R1-R6) are then used to build a microkinetic model in order to obtain detailed information on the relative rates, apparent activation barriers, and rate-controlling steps of the CO electro-oxidation on the three SFMO surface models at experimentally relevant conditions. We used a temperature range of 900 – 1300 K and partial pressures of CO and CO_2 of 1 atm and 0.03 atm, respectively. The oxygen partial pressure at the cathode is assumed to be 0.21 atm. The calculated forward rate and equilibrium constants of the

Journal of Materials Chemistry A Accepted Manuscript

elementary reactions (R1-R6) at a representative temperature of 1100 K are summarized in Table 1 and the results obtained from our microkinetic analysis without considering the effect of anode potential bias are listed in Table 2 (short circuit condition). In correlation with the free energy profiles, the microkinetic analysis also predicts a higher reaction rate and lower apparent activation barrier for the "plane-Mo" surface compared to the "diagonal-Mo" and FeO_2-terminated surfaces. The reaction rates calculated for CO oxidation on all three surfaces are however lower than the corresponding H_2 oxidation rates. Campbell's degree of rate control analysis indicates that the CO_2 formation process (R3) is mostly rate-controlling on all three surfaces. Next, the bridged-CO formation process (R2) also seems to have some effect on the overall rate when the reaction occurs on $Mo-O-Fe$ sites. Campbell's degree of thermodynamic rate control analysis furthermore reveals that the overall rate is sensitive only to the stability of the reactant structure (IM1) which is the only dominant intermediate throughout the considered temperature range.

Table 2. Calculated rates, apparent activation barriers (E_{app}), degree of rate control (X_{RC}), and degree of thermodynamic rate control (X_{TRC}) for CO oxidation on SFMO surfaces obtained from microkinetic analysis at 1100 K[a]

Surface model	Active site	Overall Rate[b] (s^{-1})	E_{app} (eV)	X_{RC} R2	X_{RC} R3	X_{TRC} $*_M$-O-Fe (IM1)
plane-Mo	$*_{Mo}$-O-Fe	2.88×10^0 (1.01×10^1)	0.99	0.3	0.7	-1.0
diagonal-Mo	$*_{Mo}$-O-Fe	1.04×10^0 (5.58×10^0)	1.39	0.1	0.9	-1.0
FeO_2-terminated	$*_{Fe}$-O-Fe	2.53×10^{-3} (5.91×10^0)	2.08	0.0	1.0	-1.0

[a] P_{CO} = 1 atm and P_{CO2} = 0.03 atm
[b] Values in parentheses correspond to the reaction rates calculated for H_2 oxidation (see Ref. 15)

Journal of Materials Chemistry A Accepted Manuscript

Next, we considered the presence of electric fields and an anode potential bias on the CO electro-oxidation mechanism since the reaction free energies of the elementary steps that involve charge transfer processes are directly affected by the potential bias. We note that the present calculations neglect the effect of electric filed which could affect the adsorption energies of different species. This is justified by the fact that all the adsorbents in the present model are neutral species which should be largely unaffected by electric fields. In contrast, the influence of an anode potential bias on the free energies of surface intermediates has to be considered for the elementary steps that involve charge transfer. For example, the Gibbs free energy for the electrochemical oxidation of CO on the SFMO surface ($CO_{(g)} + O_O^{\times}(SFMO) \rightarrow CO_{2(g)} + 2e' + V_O^{\bullet\bullet}(SFMO)$, eq 1) is calculated as

$$\Delta G = G(CO_2) + G\,(V_O^{\bullet\bullet}) + 2e\Delta V - G(CO) - G(O_O^{\times}) \qquad (2)$$

where $G(CO_2)$ and $G(CO)$ are the free energies of the CO_2 and CO gas molecules, $G\,(V_O^{\bullet\bullet})$ and $G(O_O^{\times})$ are the free energies of the SFMO surfaces with and without a surface oxygen vacancy, respectively. ΔV is the cell voltage which is the difference between the cathode potential and the anode potential ($\Delta V = V_{cathode} - V_{anode}$) and e is the magnitude of charge of an electron (1.60×10^{-19} C). At SOFC operating conditions of 800 °C, 0.21 atm cathode O_2 partial pressure, and 1 atm anode CO partial pressure, the free energy of reaction CO + ½O_2 → CO_2 is calculated as -2.2 eV.[45, 46] Because the electrochemical reactions at electrodes involve a transfer of two electrons per mole of CO, the maximum open-circuit voltage (OCV) at these conditions is 2.2/2 = 1.1 V. This serves as a reference for the electrode potential and we fix the cathode equilibrium potential to be 1.1 V.[47] In an elementary step that involves one or two electron charge transfer (we note that our microkinetic model permits charge transfer of 0, 1, or 2 e^- at every step and let the system of equations choose when and to which degree charge is transferred), the chemical

Journal of Materials Chemistry A Accepted Manuscript

potential of the product is shifted by the amount of charge multiplied by the cell voltage (ΔV). Furthermore, the activation barrier ($\Delta G_f^{0,\neq}$) of the charge transfer step also needs to be adjusted by $n_i\beta\Delta V$ and the forward (k_f) and reverse (k_r) rate constants of the charge transfer step are calculated as

$$k_f = A_f \exp\left(\frac{-\Delta G_f^{0,\neq} - n_i\beta\Delta V}{RT}\right);\ k_r = A_r \exp\left(\frac{-\Delta G_r^{0,\neq} - n_i(1-\beta)\Delta V}{RT}\right) \quad (3)$$

Here, A_f and A_r denote the frequency factors of the forward and reverse rates, respectively, n_i represents the number of transferred electrons in the charge transfer step, and β is the symmetry factor. A symmetry factor of 0 should be used for fast charge transfer occurring independent of a reaction step and 0.5 for charge transfer occurring simultaneously with a reaction step. An average value of $\beta = 0.5$ is commonly used in the literature due to a lack of information regarding the nature of the charge transfer process. We chose $\beta = 0$ in the present work assuming that the charge transfer is a fast process that can occur at any point in time which we consider most suitable for gas phase electrochemistry. However, we found that both possibilities ($\beta = 0\ or\ 0.5$) provide similar rates for the CO electro-oxidation reaction at operating voltage $\Delta V \geq 0.7$ V (Table 3) and our conclusions remain unchanged for $\beta \in [0, 0.5]$.

Table 3. Reaction rates calculated for elementary steps with and without charge transfer on the "plane-Mo" SFMO surface at a representative temperature of 1100 K and a cell voltage of 0.7 V with different symmetry factor (β) values. Bold numbers correspond to reaction rates of the preferred reaction pathways.

Reaction		**Reaction Rate (s^{-1})**	
		β = 0.0	**β = 0.5**
1. $(*_M - O - Fe)^x + CO(g) \rightarrow (CO_M - O - Fe)^x$	**(R1)**	**4.14×10^{-3}**	**4.10×10^{-3}**
2. $(*_M - O - Fe)^x + CO(g) \rightarrow (CO_M - O - Fe)^{\bullet} + e'$		1.18×10^{-7}	1.80×10^{-6}
3. $(*_M - O - Fe)^x + CO(g) \rightarrow (CO_M - O - Fe)^{\bullet\bullet} + 2e'$		3.61×10^{-11}	3.56×10^{-10}
4. $(CO_M - O - Fe)^x \rightarrow (OCO_M - Fe)^x$	**(R2)**	**4.07×10^{-3}**	**4.03×10^{-3}**

Journal of Materials Chemistry A Accepted Manuscript

5. $(CO_M - O - Fe)^x \rightarrow (OCO_M - Fe)^{\bullet} + e'$		7.11×10^{-5}	7.12×10^{-5}
6. $(CO_M - O - Fe)^x \rightarrow (OCO_M - Fe)^{\bullet\bullet} + 2e'$		4.15×10^{-7}	5.91×10^{-7}
7. $(CO_M - O - Fe)^{\bullet} \rightarrow (OCO_M - Fe)^{\bullet}$		5.43×10^{-8}	1.78×10^{-6}
8. $(CO_M - O - Fe)^{\bullet} \rightarrow (OCO_M - Fe)^{\bullet\bullet} + e'$		6.41×10^{-8}	1.47×10^{-8}
9. $(CO_M - O - Fe)^{\bullet\bullet} \rightarrow (OCO_M - Fe)^{\bullet\bullet}$		4.60×10^{-11}	3.73×10^{-10}
10. $(OCO_M - Fe)^x \rightarrow (*_M - V_O(S) - CO_{2\,(Fe)})^x$	**(R3)**	**2.03×10^{-3}**	**2.03×10^{-3}**
11. $(OCO_M - Fe)^x \rightarrow (*_M - V_O(S) - CO_{2\,(Fe)})^{\bullet} + e'$		**1.99×10^{-3}**	**1.94×10^{-3}**
12. $(OCO_M - Fe)^x \rightarrow (*_M - V_O(S) - CO_{2\,(Fe)})^{\bullet\bullet} + 2e'$		5.18×10^{-5}	6.55×10^{-5}
13. $(OCO_M - Fe)^{\bullet} \rightarrow (*_M - V_O(S) - CO_{2\,(Fe)})^{\bullet}$		1.93×10^{-5}	4.87×10^{-5}
14. $(OCO_M - Fe)^{\bullet} \rightarrow (*_M - V_O(S) - CO_{2\,(Fe)})^{\bullet\bullet} + e'$		5.18×10^{-5}	2.43×10^{-5}
15. $(OCO_M - Fe)^{\bullet\bullet} \rightarrow (*_M - V_O(S) - CO_{2\,(Fe)})^{\bullet\bullet}$		4.79×10^{-7}	6.05×10^{-7}
16. $(*_M - V_O(S) - CO_{2\,(Fe)})^x \rightarrow (*_M - V_o(S) - Fe)^{\bullet\bullet} + CO_2(g) + 2e'$	**(R4)**	**2.03×10^{-3}**	**2.03×10^{-3}**
17. $(*_M - V_O(S) - CO_{2\,(Fe)})^{\bullet} \rightarrow (*_M - V_o(S) - Fe)^{\bullet\bullet} + CO_2(g) + e'$		**2.01×10^{-3}**	**1.99×10^{-3}**
18. $(*_M - V_O(S) - CO_{2\,(Fe)})^{\bullet\bullet} \rightarrow (*_M - V_o(S) - Fe)^{\bullet\bullet} + CO_2(g)$		1.04×10^{-4}	9.04×10^{-5}
19. $(*_M - V_o(S) - Fe)^{\bullet\bullet} \rightarrow (*_M - V_o(B) - Fe)^{\bullet\bullet}$	**(R5)**	**4.14×10^{-3}**	**4.10×10^{-3}**
20. $(*_M - V_o(B) - Fe)^{\bullet\bullet} + \frac{1}{2}O_2(g) + 2e' \rightarrow (*_M - O - Fe)^x$	**(R6)**	**4.14×10^{-3}**	**4.10×10^{-3}**

In order to include the effect of anode bias potential in the CO electro-oxidation mechanism, we considered the possibility of zero, one- and two-electron charge transfer for all elementary steps (R1-R4) with the constraint that two electrons have to be transferred in the complete electro-catalytic cycle. For this extended microkinetic model, we then recalculate the surface coverages (probability density of each state) and rates. These calculations were carried out at a temperature of 1100 K and a cell voltage, ΔV, that varies from 0.1 to 1.1 V. Table 3 lists all elementary reaction steps considered for zero, one- and two-electron charge transfer and the

Journal of Materials Chemistry A Accepted Manuscript

calculated rates at a representative cell voltage of 0.7 V for the "plane-Mo" surface model. Inspection of the elementary reaction rates suggests that a two-electron charge transfer during the CO_2 desorption process (R4) and two one-electron charge transfers during steps R3 & R4 are equally favorable on the plane-Mo surface model. For a cell voltage (ΔV) between 0.1 and 1.1 V, a similar trend was observed for all three surface models considered here.

Table 4. Overall rates and degree of rate control (X_{RC}) for CO and H_2 electro-oxidation on various SFMO surfaces calculated in the presence of a typical anode bias potential.[a]

Surface model	Active site	CO oxidation		H_2 Oxidation[b]	
		Overall rate (s^{-1})	X_{RC} (CO_2 desorption)	Overall rate (s^{-1})	X_{RC} (H_2O desorption)
"plane-Mo"	$*_{Mo}$-O-Fe	4.14×10^{-3}	1.0	2.26×10^{-2}	1.0
"diagonal-Mo"	$*_{Mo}$-O-Fe	1.07×10^{-3}	1.0	4.90×10^{-3}	1.0
FeO_2-terminated	$*_{Fe}$-O-Fe	7.45×10^{-5}	1.0	2.52×10^{-4}	1.0

[a] T = 1100 K; $P_{CO(H2)}$ = 1 atm; $P_{CO2(H2O)}$ = 0.03 atm; ΔV = 0.7 V
[b] see Ref. 15

The overall rates calculated for the three surfaces at a cell voltage of 0.7 V and Campbell's degrees of rate control in the presence of the anode bias potential are summarized in Table 4. For comparison, we also provided in Table 4 the results obtained for the H_2 electro-oxidation on these surfaces from our previous work.[15] The overall rates calculated at ΔV = 0.7 V for the CO electro-oxidation are about 2-3 orders of magnitude lower than the rates at short circuit condition (ΔV = 0 V, Table 2). The "plane-Mo" surface exhibits the highest rate for both H_2 and CO electro-oxidation reactions. Figure 3 shows the effect of cell voltage on the overall rate, i.e., simulated polarization curves (cell voltage versus current density) in the absence of any resistances but for those from anode reactions. The current density (i in Acm^{-2}) is calculated using the relation, $i = zer\Gamma$, where z is the number of electron(s) involved in the reaction, r

Journal of Materials Chemistry A Accepted Manuscript

represents the calculated overall reaction rate (s^{-1}), and Γ is the number of active sites per surface area (cm^{-2}). We highlight that we assume here that there are no Ohmic losses or mass transfer limitations, which is somewhat justified at low currents since the cell is operating at a high temperature and SFMO is an excellent electron and ion conductor. Under relevant operating conditions, however, Ohmic losses and mass transfer limitations will also affect the cell performance and our analysis cannot quantitatively predict experimental cell behavior. Nevertheless, the calculated current densities can be used to compare the activity of different surface models for the same electro-oxidation reaction or compare different electro-oxidation reactions on the same surface model. The simulated polarization curves clearly demonstrate that the CO electro-oxidation activity is higher on Mo sites than Fe site at all cell voltages from short-circuit to open-circuit conditions. At lower cell voltages (ΔV = 0.1-0.4 V), the calculated current density on the FeO_2-terminated surface is about 3 orders of magnitude lower than that of the "plane-Mo" surface and this difference becomes smaller at operating voltage ($\Delta V \geq 0.7$ V). This trend suggests a change in rate-limiting step on these surfaces when the cell voltage increases from 0.1 to 0.7 V. Accordingly, a Campbell's degree of rate control analysis suggests that the CO_2 desorption process, which is the surface oxygen vacancy formation process as well as the charge transfer process, is the rate-controlling step on all the three surfaces at SOFC operating voltages of $\Delta V \geq 0.7$ V (Table 4). In contrast, at short-circuit condition (Table 2) and low cell voltage the CO_2 formation process is rate controlling. The larger difference in the CO oxidation activity on the FeO_2-terminated surface compared to the "plane-Mo" surface at low cell voltage conditions is due to a large difference in CO_2 formation barrier (TS3, Figure 2) on these two surfaces. In other words, the "surface diffusion" of CO is more difficult on the FeO_2-terminated surface compared to the surfaces with Mo in the top surface layer. On the other hand, at higher

Journal of Materials Chemistry A Accepted Manuscript

cell voltage conditions, the vacancy formation free energy difference between these two surfaces (IM5, Figure 2) is much smaller and thus, the activity difference also becomes smaller.

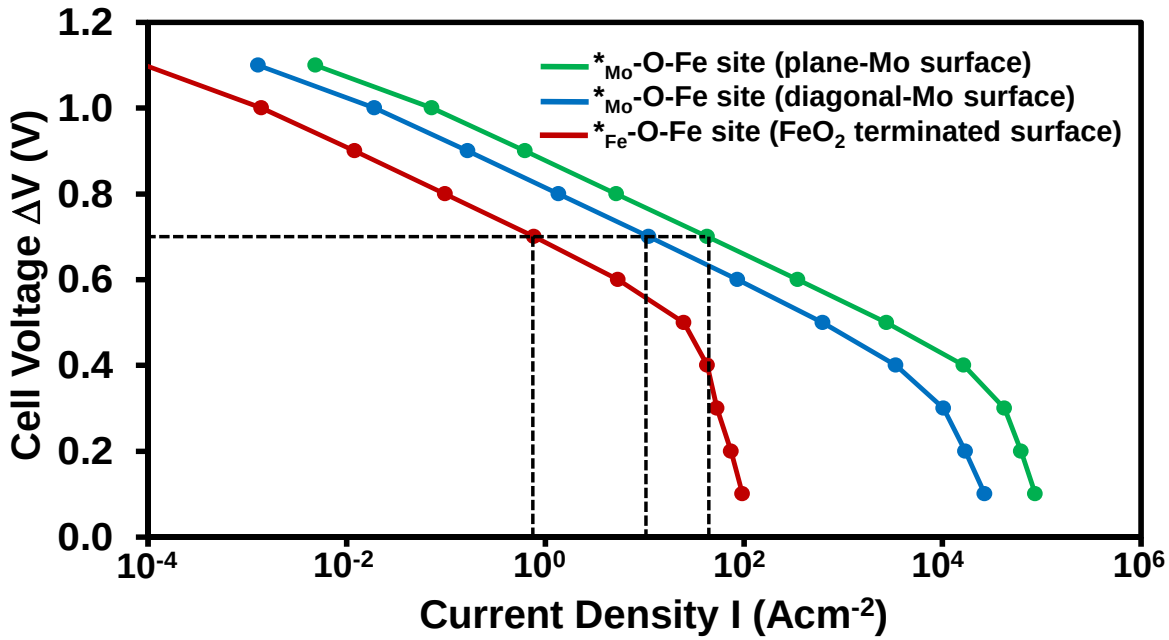

Figure 3. Calculated polarization curves (current per surface area of the individual surface models) for CO electro-oxidation on SFMO (001) surfaces (T = 1100 K). Dashed line indicates the current density at an operating voltage of 0.7 V.

In case of the H_2 electro-oxidation,[15] we also identified a change in rate-controlling steps, i.e., H_2 dissociation and H_2O formation are rate-controlling at low cell voltage and H_2O desorption becomes rate-controlling at higher cell voltage on all three surface models. However, at short circuit condition, the calculated current densities on the three surface models were very similar and they differed significantly only at higher cell voltage conditions. This suggests that the surface diffusion of hydrogen is very similar on the three surface models unlike the surface CO diffusion which is facilitated by the presence of Mo. Since the H_2O desorption process, which also corresponds to the surface oxygen vacancy formation as well as the charge transfer process, is rate-controlling at higher cell voltage conditions, the H_2 electro-oxidation activity difference between the three surface models is very similar to the CO electro-oxidation activity

Journal of Materials Chemistry A Accepted Manuscript

difference (Table 4). The high barriers associated with the surface diffusion of CO compared to hydrogen could possibly contribute more to the overall lower rates calculated for the CO electro-oxidation compared to the H_2 electro-oxidation on each surface model. Our findings seem to be in correlation with the reported results for H_2 and CO electro-oxidation on Ni-based anodes. It has been shown in the literature[7, 8, 11-13] that the electrochemical reaction rate of CO on different types of Ni anodes, such as nickel-pattern anodes, nickel-point anodes, and Ni-YSZ porous anodes is lower than that of H_2. These studies reported that in the presence of pure CO, the maximum power density reaches only about 40-50% of that obtained with pure H_2. A combination of slow CO electrochemical kinetics and a lower diffusivity of the relatively heavy CO molecules were suggested to be responsible for the observed lower power density for CO fuel. In addition, it has been shown that the kinetics of the CO electro-oxidation has a positive reaction order with respect to CO partial pressure when using Ni-YSZ[6, 11] or Cu-CeO_2-YSZ[6] anodes. Jiang and Virkar[11] found that the maximum power density of SOFC with a Ni-YSZ anode decreases by 60% when P_{CO} was decreased from 1 to 0.44 atm when diluting with CO_2 at 1073 K whereas Costa-Nunes et al.[6] reported a 27% decrease in the maximum power density when using a Cu-CeO_2-YSZ anode and decreasing the CO pressure from 1 to 0.5 atm by diluting in CO_2 at 973 K. Our computations on the SFMO surface predict a reaction order of 1.0 with respect to CO and zero with respect to CO_2 on all surface models at a cell voltage of 0.7 V and 1100 K. We find that the overall rate of CO electro-oxidation on all three surface models decreased by 50% when using P_{CO} = 0.5 atm and P_{CO2} = 0.5 atm in our microkinetic model.

The promotional effect of surface Mo on the H_2 electro-oxidation activity has been discussed in our earlier work.[15] The rate-controlling surface oxygen vacancy formation was found to be facilitated on the surface with higher Mo concentration on the gas exposed layer. On

Journal of Materials Chemistry A Accepted Manuscript

the other hand, our *ab initio* thermodynamic analysis suggested that the Mo concentration on the SFMO surface will be very low and the least active FeO_2-terminated surface is the stable surface under SOFC anodic conditions. A combination of our thermodynamic analysis and kinetic studies helped us to explain the experimentally observed poor activity of this material. In agreement with the experimental observation that the performance of this material can be improved by dispersing a small amount of Ni (~ 2 wt%) into the SFMO anode,[21] we also found that adding small Ni clusters to the FeO_2-terminated surface dramatically reduces the surface oxygen vacancy formation energy[15, 48] which improves the activity of this surface. Furthermore, Bader charge analysis[49, 50] on the initial catalyst surface models suggested that the Mo atoms on the top layer of the "plane-Mo" surface were in a high oxidation state Mo^{6+} (formal charges) due to the presence of only two oxygen vacancies, whereas on the FeO_2-terminated surface, the surface Fe atoms were already reduced to Fe^{2+} (formal charges) state due to the presence of four oxygen vacancies. Thus, it was easier to remove an oxygen from the $Mo - O - Fe$ site during the catalytic cycle because the extra charge left can be transferred to the neighboring Mo^{6+} atom. However, removing an oxygen from the $Fe - O - Fe$ site reduced Fe from its stable Fe^{2+} state to an unstable Fe^{1+} state and hence destabilized the vacancy structure. When Ni was present on this surface, the extra charge was transferred to Ni without further reducing the Fe^{2+} atoms. Thus, the rate-controlling vacancy formation was promoted by the presence of Mo and Ni, both able to receive the extra charge left by the oxygen removal process. The same analysis can also be used to understand the promotional effect of Mo on the CO electro-oxidation activity of the SFMO surfaces since the rate-controlling process is here again the surface oxygen vacancy formation process. As a result, we hypothesize that the CO electro-oxidation activity of the FeO_2-terminated surface can again be improved by adding small Ni particles.

Journal of Materials Chemistry A Accepted Manuscript

3.2. Syngas electro-oxidation on the SFMO (001) surfaces.

The presence of both H_2 and CO in the fuel stream complicates the reaction mechanism since electrochemical H_2 and CO electro-oxidation reactions can occur in parallel to the non-electrochemical (i.e., chemical) water-gas shift reaction. We highlight that an advantage of our multiscale modeling strategy is that the system of equations determines by itself if a chemical or electro-chemical reaction with charge transfer occurs. The activity of Ni/YSZ anodes in the presence of H_2 and CO mixtures have been examined earlier.[6-14] These experimental studies with different types of Ni anodes reported a very similar cell performance when using H_2 and CO mixtures in comparison to pure H_2 fuel, even when the CO concentration is as high as 55%, suggesting that CO played a minimal role in the overall electrochemical oxidation rates. A decrease in the cell performance was observed only at high CO content (>90%). Since the H_2 electrochemical oxidation is faster, the presence of excess H_2 does not permit significant CO electro-oxidation. Instead, CO can effectively be converted to H_2 via the WGS reaction ($CO + H_2O \rightleftharpoons CO_2 + H_2$) which again can be electro-oxidized. Thus, the electrochemical activity is maintained even at a relatively high CO content. While these studies provide some understanding on the behavior of Ni anodes in the presence of syngas fuel with different compositions, very little is known about the performance of alternative anodes with syngas fuel. In the following, we used a similar computational approach as described in Section 2 to investigate the syngas (electro-)oxidation on the three SFMO surface models. The elementary steps of the H_2 and CO electro-oxidation reactions and the WGS reaction, as illustrated in Figure 4, are included in the microkinetic model and the cell voltage ΔV is varied from 0.1 V to 1.1 V. The partial pressures of H_2O and CO_2 are fixed at 0.03 and 0.003 atm, respectively, and different

Journal of Materials Chemistry A Accepted Manuscript

partial pressures of H_2 and CO are considered in the microkinetic analysis. We choose a wet (3% H_2O) fuel condition for the current analysis because (1) water is produced during the H_2 electro-oxidation and (2) it has been shown earlier for Ni-YSZ anodes operating on dry syngas fuels that only the H_2 component of the fuel is utilized.[6, 11]

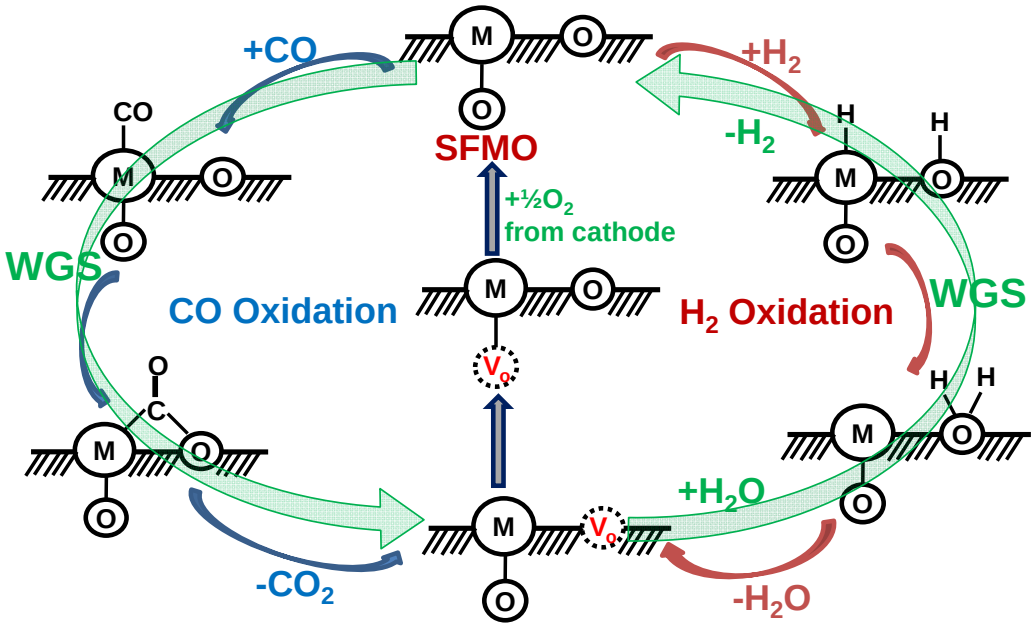

Figure 4. Proposed mechanism for syngas oxidation on $Sr_2Fe_{1.5}Mo_{0.5}O_{6-\delta}$ (SFMO) surface.

The individual reaction rates calculated with $P_{H2}=P_{CO}=0.5$ atm at different cell voltages are listed in Table 5. At lower cell voltage conditions (e.g. $\Delta V=0.3$ V), the H_2 electro-oxidation is the dominant process on all surface models. On the "plane-Mo" surface, the rates calculated for the CO electro-oxidation and the WGS reaction are very similar and are only slightly lower than the H_2 electro-oxidation rate. However, the CO electro-oxidation rate is about 1-2 orders of magnitude lower than the H_2 electro-oxidation rate on the other two surfaces. Due to the high CO_2 formation barrier (Figure 2) on the FeO_2-terminated surface, the CO electro-oxidation (left side of Figure 4) and the WGS are much less favorable than the H_2 electro-oxidation (right side of Figure 4). Such a fast electro-oxidation of H_2 compared to CO and the WGS at low cell

Journal of Materials Chemistry A Accepted Manuscript

voltage conditions leads to surface coverage conditions that promote the *reverse* WGS reaction. We only observed occurrence of the *reverse* WGS (instead of the WGS) at conditions when the H_2 electro-oxidation is about two orders of magnitude faster than the WGS at open cell conditions. At higher cell voltage conditions ($\Delta V \geq 0.7$ V), the H_2 electro-oxidation slows down and the WGS becomes the dominant process on all three surface models. The higher WGS rate predicted for the "plane-Mo" surface is due to its lower oxygen vacancy formation energy as well as easier diffusion of both hydrogen and CO on the surface compared to the "diagonal-Mo" and FeO_2-terminated surfaces. At a cell voltage of 0.7 V about 80% of the current originates from H_2 electro-oxidation independent of the surface Mo concentration.

Table 5. Calculated reaction rates for CO and H_2 electro-oxidation reactions and water-gas shift (WGS) on the SFMO surfaces with different Mo concentration in the presence of a syngas fuel at various cell voltages (ΔV).[a] The rate of the dominant reaction at a particular cell voltage is shown in bold number.

Surface model	Reaction	Reaction Rate (s^{-1})		
		ΔV = 0.3 V	**ΔV = 0.7 V**	**ΔV = 1.0 V**
"plane-Mo" ($*_{Mo}$-O-Fe)	H_2 electro-oxidation	$\mathbf{1.39 \times 10^{1}}$	1.08×10^{-2}	1.71×10^{-5}
	CO electro-oxidation	1.40×10^{0}	2.03×10^{-3}	3.58×10^{-6}
	WGS reaction	8.13×10^{-1}	$\mathbf{1.28 \times 10^{0}}$	$\mathbf{1.28 \times 10^{0}}$
"diagonal-Mo" ($*_{Mo}$-O-Fe)	H_2 electro-oxidation	$\mathbf{2.49 \times 10^{0}}$	1.39×10^{-3}	2.22×10^{-6}
	CO electro-oxidation	2.56×10^{-1}	2.97×10^{-4}	9.67×10^{-7}
	WGS reaction	3.36×10^{-1}	$\mathbf{4.23 \times 10^{-1}}$	$\mathbf{4.23 \times 10^{-1}}$
FeO_2-terminated ($*_{Fe}$-O-Fe)	H_2 electro-oxidation	$\mathbf{3.94 \times 10^{-1}}$	8.68×10^{-5}	1.36×10^{-7}
	CO electro-oxidation	7.87×10^{-3}	2.26×10^{-5}	9.37×10^{-7}
	WGS reaction	-5.34×10^{-3}	$\mathbf{1.14 \times 10^{-3}}$	$\mathbf{1.14 \times 10^{-3}}$

[a] T = 1100 K; P_{H2} = 0.5 atm; P_{CO} = 0.5 atm; P_{H2O} = 0.03 atm; ; P_{CO2} = 0.003 atm

Journal of Materials Chemistry A Accepted Manuscript

In order to further examine how the concentration of H_2 and CO in the fuel mixture affects the overall activity of an SFMO anode, we simulated polarization curves (under the approximations mentioned above) with different partial pressures of H_2 and CO. Figure 5 illustrates the calculated polarization curves with three different syngas compositions; (i) P_{H2}= 0.85 atm and P_{CO} = 0.15 atm, (ii) P_{H2}= 0.50 atm and P_{CO} = 0.50 atm, and (iii) P_{H2}= 0.15 atm and P_{CO} = 0.85 atm. The partial pressures of H_2O and CO_2 have been kept constant at 0.03 and 0.003 atm, respectively. For comparison, we also included in this figure the polarization curves calculated for pure H_2 and pure CO. The individual reaction rates calculated at representative cell voltages of 0.3 V, 0.7 V, and 1.0 V are summarized in the supporting information (Tables S2) and Table 5. On all surface models, the calculated current densities with a H_2 and CO fuel mixture at operating voltage ($\Delta V \geq 0.7$ V) are very similar to those of the pure H_2 fuel as long as the CO content is below 50%. This observation is consistent with the reported experimental results for the Ni-YSZ anode discussed above. Under these conditions the WGS reaction is very rapid and the H_2 electro-oxidation is the dominant electrochemical process. We find that in general, whenever the H_2 content is high (and the CO content is low), the H_2 electro-oxidation is the dominant electrochemical process and the polarization curve is very similar to the polarization curve with pure H_2. At these low CO content conditions, we find that a higher H_2 partial pressure leads at fixed operating voltage to a higher current. When the CO content is increased to 85%, the current density slightly decreases on the "plane-Mo" surface, but in general remains still significantly higher than the current density calculated for pure CO fuel. Since the current density calculated for pure H_2 fuel is about an order of magnitude higher than that of pure CO fuel on this surface, the dominant electro-oxidation process remains the H_2

Journal of Materials Chemistry A Accepted Manuscript

electro-oxidation process at all operating voltages even when the CO content is as high as 85%. In contrast, at a high CO content of 85% and at (high) operating voltage, the "diagonal-Mo" and FeO_2-terminated surfaces display an activity as if the feed stream would consist of pure CO. The individual reaction rates provided in Table S2 suggest that the CO electro-oxidation contributes more to the current on these two surfaces at these conditions. This observation can be explained by the rate controlling step in the H_2 and CO electro-oxidation being very similar at these conditions (the formation of an oxygen vacancy) and since the CO partial pressure is larger than the H_2 pressure, performance can be dominated by the CO electro-oxidation. At low cell voltage, the rate-controlling step shifts away from oxygen vacancy formation, the H_2 electro-oxidation becomes significantly faster than the CO electro-oxidation and the current-voltage characteristic is again similar to the scenarios with higher H_2 content. Overall, these results suggest that when using syngas fuels, the electrochemical activity of SFMO anodes originates primarily from the H_2 electro-oxidation, while CO is chemically shifted via the WGS. The "plane-Mo" surface is furthermore even very active for syngas fuels with a high CO content.

Journal of Materials Chemistry A Accepted Manuscript

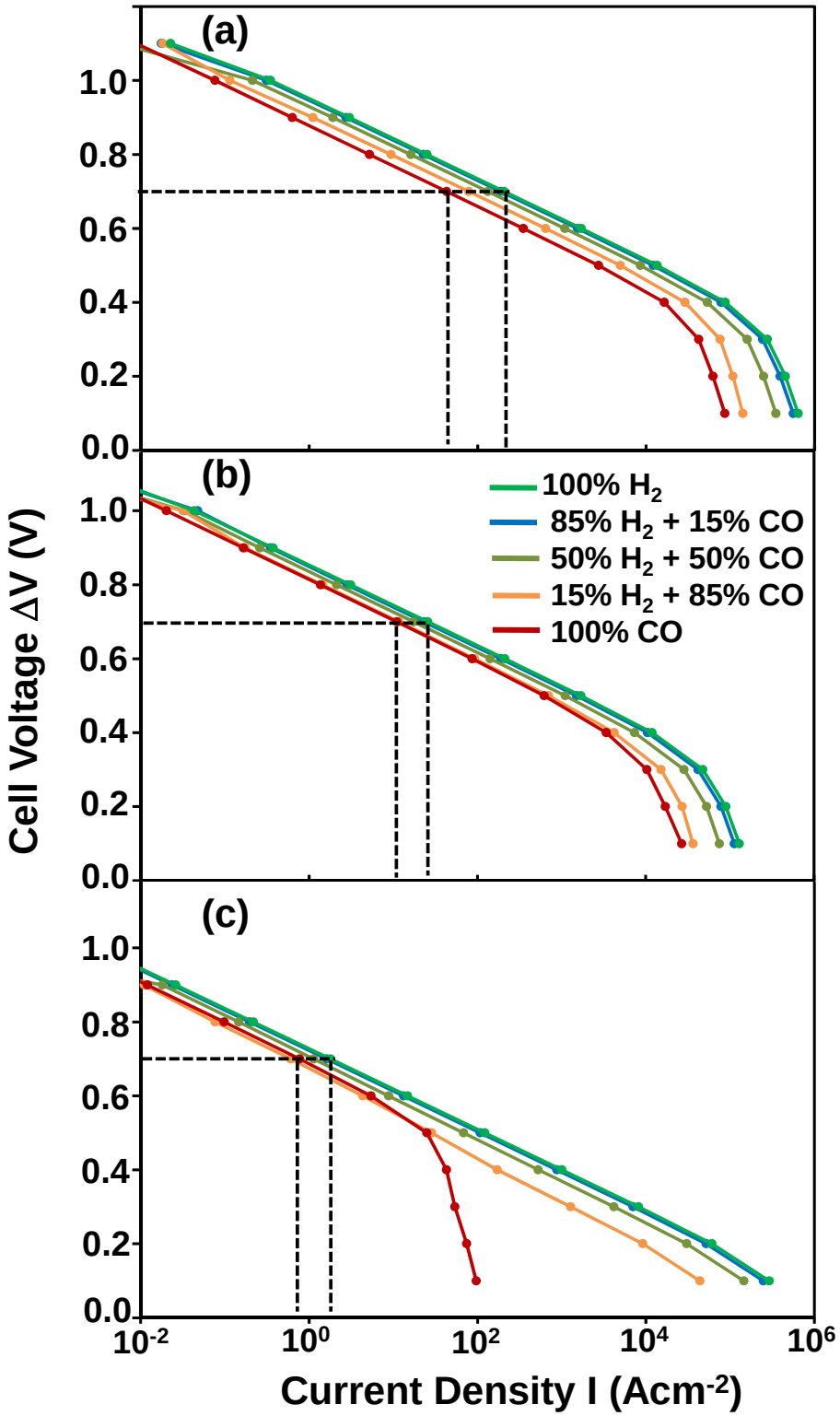

Figure 5. Calculated polarization curves for syngas oxidation on various SFMO (001) surfaces (a) "plane-Mo" surface (b) "diagonal-Mo" surface (c) FeO_2-terminated surface (T = 1100 K). Dashed lines indicate the current density at an operating voltage of 0.7 V.

Journal of Materials Chemistry A Accepted Manuscript

4. Conclusions

We investigated the activity of SFMO anode electrodes in the presence of CO and syngas fuels using DFT+U theory and microkinetic modeling techniques. Three SFMO (001) surface models with varying concentration of Mo and oxygen vacancies on the gas exposed surface layer, identified from our earlier *ab initio* thermodynamic analysis, were considered for this study. Kinetic analysis, including the effect of anode bias potential, suggested that the "plane-Mo" surface with a high Mo concentration in the top surface layer is more active for the CO electro-oxidation that the "diagonal-Mo" and FeO_2-terminated surfaces. We identified a similar trend in the activity of these surfaces for the H_2 electro-oxidation in our earlier work. The CO electro-oxidation activity on all surfaces is lower than their corresponding H_2 electro-oxidation activity. Campbell's degree of rate control analysis suggested that the surface diffusion of CO is rate-controlling at low cell voltage conditions whereas the desorption of CO_2, which creates a surface oxygen vacancy and is also the charge-transfer step, is rate-controlling at operating voltage. As already found earlier in the H_2 electro-oxidation mechanism, the CO electro-oxidation activity of the SFMO surface can be correlated to the ability to form surface oxygen vacancies under SOFC operating conditions. The "plane-Mo" surface has a lower surface oxygen vacancy formation energy and is more active for CO electro-oxidation than the most stable FeO_2-terminated surface. Thus, SFMO perovskite oxide is expected to exhibit a relatively poor catalytic activity for CO electro-oxidation (similar to the experimental observation made for the H_2 electro-oxidation). However, the CO electro-oxidation activity can be improved either by increasing the Mo content or adding an active transition metal to the SFMO surface.

When both CO and H_2 are present in the fuel stream (syngas), we found that the SFMO anode exhibits a similar behavior to Ni-based anodes, i.e., the activity in the presence of a H_2 and

Journal of Materials Chemistry A Accepted Manuscript

CO mixture is very similar to that of pure H_2 fuel as long as the CO content is below 50% at operating voltage ($\Delta V \geq 0.7$ V). At a higher CO content, the activity of the "plane-Mo" surface only slightly decreases and remains still higher than the activity observed for pure CO fuel. However, when the CO content is increased to 85%, the "diagonal-Mo" and FeO_2-terminated surfaces exhibit a similar activity to that observed of pure CO fuel. At a lower cell voltage, we find that the H_2 electro-oxidation is the dominant process, whereas at operating voltage the WGS reaction becomes rapid on the three surface models. Similar to observations for Ni-based anodes, it is primarily the H_2 electro-oxidation that contributes to the overall electrochemical activity of SFMO anodes when using syngas fuel and CO is primarily chemically shifted via the WGS reaction. Next, increasing the surface Mo content would improve the activity of SFMO anodes for syngas fuels of all CO concentrations. Finally, our results more generally suggest that any process more "difficult" than hydrogen electro-oxidation on a SOFC anode surface is likely a chemical and not an electro-chemical process (as CO oxidation in the presence of water is primarily a chemical oxidation rather than an electro-chemical oxidation). In other words, considering the difficulty in splitting C-H bonds in hydrocarbon fuels, it is likely that in SOFCs operating on various hydrocarbon fuels and in the presence of water, it is only the adsorbed hydrogen that is electro-oxidized while all other processes are chemical in nature. A more detailed discussion of methane electro-oxidation and carbon deposition will be addressed in a future study.

Acknowledgements

This work was supported by the Heterogeneous Functional Materials Center (HeteroFoaM), an Energy Frontier Research Center (EFRC) funded by the U.S. Department of

Journal of Materials Chemistry A Accepted Manuscript

Energy, Office of Basic Energy Science under Award No. DE-SC0001061. Computations were carried out at the U.S. Department of Energy facilities located at the National Energy Research Scientific Computing Center (NERSC) and at EMSL, located at Pacific Northwest National Laboratory (Grant Proposal 47883). Furthermore, a portion of this research was performed with XSEDE resources provided by the National Institute for Computational Sciences (NICS) and Texas Advanced Computing Center (TACC) under grant number TG-CTS090100. Finally, computing resources from USC's High Performance Computing Group are gratefully acknowledged.

Notes

Electronic Supplementary Information (ESI) available: 1.Details of surface model development, 2. Microkinetic model, Table S1 (Reaction energies and activation barriers for the elementary steps considered for the CO oxidation), Table S2 (Reaction rates calculated for the CO and H_2 electro-oxidation reactions and water-gas shift reaction in the presence of syngas fuel with different gas compositions), Figures S3 & S4 (Intermediates and transition state structures involved in the CO oxidation reaction on the "diagonal-Mo" surface and FeO_2 terminated surface, respectively).

References

1. S. C. Singhal and K. Kendall, *High temperature solid oxide fuel cells: fundamentals, design and applications.*, Elsevier, Oxford, UK, 2003.
2. M. Li, A. D. Rao, J. Brouwer and G. S. Samuelsen, *J. Power Sources*, 2010, **195**, 5707-5718.
3. A. Verma, A. D. Rao and G. S. Samuelsen, *J. Power Sources*, 2006, **158**, 417-427.
4. J. Hanna, W. Y. Lee, Y. Shi and A. F. Ghoniem, *Prog. Energy Combust. Sci.*, 2014, **40**, 74-111
5. J. Hanna, W. Y. Lee and A. F. Ghoniem, *J. Electrochem. Soc.*, 2013, **160**, F698-F708.
6. O. Costa-Nunes, R. J. Gorte and J. M. Vohs, *J. Power Sources*, 2005, **141**, 241-249.
7. Y. Matsuzaki and I. Yasuda, *J. Electrochem. Soc.*, 2000, **147**, 1630-1635.

Journal of Materials Chemistry A Accepted Manuscript

8. A. M. Sukeshini, B. Habibzadeh, B. P. Becker, C. A. Stoltz, B. W. Eichhorn and G. S. Jackson, *J. Electrochem. Soc.*, 2006, **153**, A705-A715.
9. R. Suwanwarangkul, E. Croiset, E. Entchev, S. Charojrochkul, M. D. Pritzker, M. W. Fowler, P. L. Douglas, S. Chewathanakup and H. Mahaudom, *J. Power Sources*, 2006, **161**, 308-322.
10. J. S. O'Brien and J. B. Giorgi, *J. Power Sources*, 2012, **200**, 14-20.
11. Y. Jiang and A. V. Virkar, *J. Electrochem. Soc.*, 2003, **150**, A942-A951.
12. K. Eguchi, H. Kojo, T. Takeguchi, R. Kikuchi and K. Sasaki, *Solid State Ionics*, 2002, **152**, 411-416.
13. K. Sasaki, Y. Hori, R. Kikuchi, K. Eguchi, A. Ueno, H. Takeuchi, M. Aizawa, K. Tsujimoto, H. Tajiri, H. Nishikawa and Y. Uchida, *J. Electrochem. Soc.*, 2002, **149**, A227-A233.
14. A. Weber, B. Sauer, A. C. Muller, D. Herbstritt and E. Ivers-Tiffee, *Solid State Ionics*, 2002, **152**, 543-550.
15. S. Suthirakun, S. C. Ammal, A. B. Muñoz-García, G. Xiao, F. Chen, H.-C. zur Loye, E. A. Carter and A. Heyden, *J. Am. Chem. Soc.*, 2014, **136**, 8374-8376.
16. Q. Liu, X. Dong, G. Xiao, F. Zhao and F. Chen, *Adv. Mater.*, 2010, **22**, 5478-5482.
17. G. Xiao and F. Chen, *Electrochem. Commun.*, 2011, **13**, 57-59.
18. A. B. Munoz-Garcia, D. E. Bugaris, M. Pavone, J. P. Hodges, A. Huq, F. Chen, H.-C. zur Loye and E. A. Carter, *J. Am. Chem. Soc.*, 2012, **134**, 6826-6833.
19. A. B. Munoz-Garcia, M. Pavone, A. M. Ritzmann and E. A. Carter, *Phys. Chem. Chem. Phys.*, 2013, **15**, 6250-6259.
20. G. Xiao, Q. Liu, S. Nuansaeng and F. Chen, *ECS Trans.*, 2012, **45**, 355-362.
21. G. L. Xiao, C. Jin, Q. Liu, A. Heyden and F. L. Chen, *J. Power Sources*, 2012, **201**, 43-48.
22. G. Kresse and J. Furthmuller, *Phys. Rev. B*, 1996, **54**, 11169-11186.
23. G. Kresse and D. Joubert, *Phys. Rev. B*, 1999, **59**, 1758-1775.
24. P. Hohenberg and W. Kohn, *Phys. Rev. B*, 1964, **136**, B864-&.
25. W. Kohn and L. J. Sham, *Phys. Rev.*, 1965, **140**, A1133.
26. V. I. Anisimov, J. Zaanen and O. K. Andersen, *Phys. Rev B*, 1991, **44**, 943-954.
27. V. I. Anisimov, F. Aryasetiawan and A. I. Lichtenstein,. *J. Phys-Condens. Mat.*, 1997, **9**, 767-808.
28. J. P. Perdew, K. Burke and M. Ernzerhof, *Phys. Rev. Lett.*, 1996, **77**, 3865-3868.
29. P. E. Blochl, *Phys. Rev. B*, 1994, **50**, 17953-17979.
30. H. J. Monkhorst and J. D. Pack, *Phys. Rev. B*, 1976, **13**, 5188-5192.
31. G. Makov and M. C. Payne, *Phys. Rev. B*, 1995, **51**, 4014-4022.
32. A. B. Munoz-Garcia, M. Pavone and E. A. Carter, *Chem. Mater.*, 2011, **23**, 4525-4536.
33. G. Henkelman, B. P. Uberuaga and H. Jonsson, *J. Chem. Phys.*, 2000, **113**, 9901-9904.
34. A. Heyden, A. T. Bell and F. J. Keil, *J. Chem. Phys.*, 2005, **123**, 224101.
35. G. Henkelman and H. Jonsson, *J. Chem. Phys.*, 1999, **111**, 7010-7022.
36. R. A. Olsen, G. J. Kroes, G. Henkelman, A. Arnaldsson and H. Jonsson, *J. Chem. Phys.*, 2004, **121**, 9776-9792.
37. A. A. Peterson, F. Abild-Pedersen, F. Studt, J. Rossmeisl and J. K. Norskov, *Energ. Environ. Sci*, 2010, **3**, 1311-1315.
38. S. C. Ammal and A. Heyden, *ACS Catal.*, 2014, **4**, 3654-3662.
39. G. Buzzi-Ferraris, Politecnico di Milano, "BzzMath: Numerical libraries in C++",

Journal of Materials Chemistry A Accepted Manuscript

www.chem.polimi.it/homes/gbuzzi <http://www.chem.polimi.it/homes/gbuzzi>.
40. C. Stegelmann, A. Andreasen and C. T. Campbell, *J. Am. Chem. Soc.*, 2009, **131**, 13563-13563.
41. C. Stegelmann, A. Andreasen and C. T. Campbell, *J. Am. Chem. Soc.*, 2009, **131**, 8077-8082.
42. S. Kozuch and S. Shaik, *J. Am. Chem. Soc.*, 2006, **128**, 3355-3365.
43. S. Kozuch and S. Shaik, *J. Phys. Chem. A*, 2008, **112**, 6032-6041.
44. F. A. Kroger and H. J. Vink, *Solid State Phys.*, 1956, **3**, 307-435.
45. P. W. Atkins, *Physical Chemistry*, Oxford University Press, Oxford, sixth edn., 1998.
46. NIST, Chemistry WebBook, http://webbook.nist.gov/chemistry).
47. J. Mukherjee and S. Linic, *J. Electrochem. Soc.*, 2007, **154**, B919-B924.
48. E. Walker, S. C. Ammal, S. Suthirakun, F. Chen, G. A. Terejanu and A. Heyden, *J. Phys. Chem. C*, 2014, **118**, 23545-23552.
49. R. F. W. Bader, *Atoms in Molecules - A quantum theory*, Oxford University Press, New York, 1990.
50. W. Tang, E. Sanville and G. Henkelman, *J. Phys-Condens. Mat*, 2009, **21**, 084204.

Journal of Materials Chemistry A Accepted Manuscript

TOC Graphics:

Concurrent simulation of chemical and electro-chemical processes on $Sr_2Fe_{1.5}Mo_{0.5}O_{6-\delta}$ predicted a higher activity for CO/syngas fuels for a surface with higher Mo content.

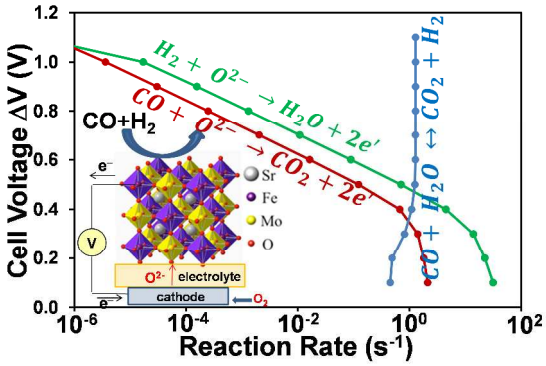

Journal of Materials Chemistry A Accepted Manuscript